Bistability Controlled by Convection in a Pattern-Forming System

Nicolas Marsal,[1,2,*] Lionel Weicker,[1,2] Delphine Wolfersberger,[1,2] and Marc Sciamanna[1,2]
[1]LMOPS, OPTEL Research Group, CentraleSupélec, Université Paris-Saclay, 57070 METZ, France
[2]LMOPS, CentraleSupélec, Université de Lorraine, 57070 METZ, France
(Received 20 July 2016; published 5 January 2017)

We analyze the transition from convective to absolute dynamical instabilities in a nonlinear optical system forming patterns, i.e., a photorefractive crystal in a single feedback configuration. We demonstrate that the convective regime is directly related to the bistability area in which the homogeneous steady state coexists with a pattern solution. Outside this domain, the system exhibits either a homogeneous steady state or an absolute dynamical regime. We evidence that the bistability area can be greatly increased by adjusting the mirror tilt angle and/or by applying an external background illumination on the photorefractive crystal.

DOI: 10.1103/PhysRevLett.118.013902

A common laser beam propagating through a nonlinear medium may become unstable against modulation instability resulting in the appearance of correlated satellite beams called pattern [1]. For its potential application in optical memories, spontaneous pattern formation has been studied in a large variety of nonlinear optical systems including optical ring or Fabry-Perot resonators filled with active or passive medium [2] and single feedback configurations using liquid crystals [3], atomic vapors [4,5], and photorefractive crystals [6,7].

One of the generic features of the previous pattern-forming systems is the subcritical bifurcation from which the pattern may originate. The bifurcation being subcritical, the pattern branch coexists with the homogeneous solution within a given range of the system parameters [8]. Among the different parameters, Odoulov *et al.* reported that the bistability can be controlled by modifying the distance between the mirror and the photorefractive crystal in a single feedback experiment [9]. In optical resonators, the cavity detuning corresponding to a mistuning between the driving wavelength and the resonance peak of the cavity has been used to adjust the bistable area [10].

Finally, it is worth noting that the bistability mechanism is possibly related to observation of localized structures that are connecting fronts between pattern and homogeneous solutions [11]. It consists of localized intensity peaks in an otherwise homogenous background that can be switched on and off at will. Therefore, being able to control the range of parameters where such localized structures may exist is crucial for their applications in all-optical information processing [12,13].

Recent preliminary work from our group in an optical system composed of a bulk photorefractive crystal subjected to a single optical feedback [14] has shown the possibility to increase the bistability between pattern and homogeneous solutions by playing with the misalignment of the feedback mirror. The bistability area becomes larger with respect to larger mirror misalignments. Reference [14] left, however, unanswered the origin of this observation and the underlying physical mechanisms. In this Letter, we demonstrate the role of the convection in the bifurcation scenario. We show the interplay between drift induced instabilities and bistability. Consequently, the bistability can be controlled and greatly enhanced by an intentional misalignment of the mirror, hence inducing the transition towards convective or even absolute dynamical instabilities. We further report on the influence of an external background illumination applied to our photorefractive crystal. Importantly, the system described by our model is fairly generic as it represents two beams counterpropagating in a saturable medium. Therefore, it is worth mentioning that our numerical and experimental observations in photorefractive materials could be of great interest in other broad area systems (VCSEL's, liquid crystal, Kerr media).

Our experimental setup is sketched in Fig. 1 and is similar to Refs. [14,15]. The system is aligned such that it induces a photorefractive two-wave mixing in a reflection-grating geometry. A p-polarized 532 nm laser beam is focused to a 300-μm diameter inside a cobalt-doped barium titanate crystal ($BaTiO_3$). The lens $L1$ fixes the input beam size. The feedback mirror can be precisely moved longitudinally and transversally to create an advectionlike effect giving rise to a transverse shift (H) between the forward (F) and the backward beam (B) (Fig. 1). Transverse patterns arising onto the backward beam trajectory are monitored in near- and far-field (Fourier transformed) thanks to the lens $L2$ and different beam splitters (BS). It is worth noting that the input intensity of the pump laser beam modifies the gain of the (nonlocal) reflection grating arising in the crystal due to the nonlinear two-wave mixing process [16]. Thus, by keeping the input beam diameter constant and only by changing the power of the laser, we can adjust carefully the nonlinear photorefractive coupling strength. This action can be enhanced by the presence of an external background illumination similar to Ref. [9]. Such an illumination can be

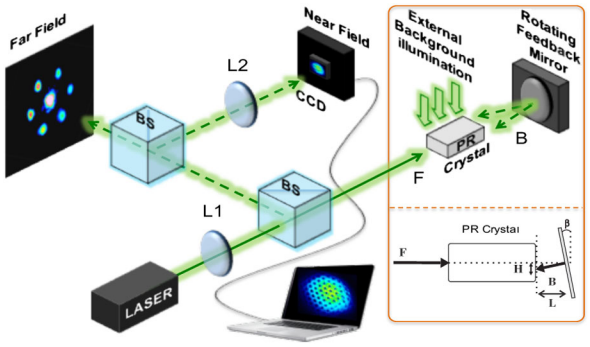

FIG. 1. Schematic of our photorefractive single feedback system. The forward (F) and backward (B) beams are responsible for the pattern formation. Lens ($L2$) and different beam splitters (BS) are used to monitor the transverse patterns arising onto the backward beam trajectory. L: distance between the mirror and the crystal, β: mirror tilt angle, $H = L.\sin(\beta)$: transverse shift (in μm).

switched on or off (Fig. 1) and is used to ensure a dependence between the photorefractive gain and the probe beam intensity, i.e., to avoid the saturation of the two-wave mixing gain for high input powers.

A simplified model describing our system has been suggested by Sandfuch *et al.* [17]. The equations are written

$$\frac{\partial F}{\partial z} + iD\Delta_\perp F = -QB, \tag{1}$$

$$-\frac{\partial B}{\partial z} + iD\Delta_\perp B = Q^* F, \tag{2}$$

$$\tau\frac{\partial Q}{\partial t} + Q = \gamma\frac{FB^*}{|F|^2 + |B|^2 + I_d}, \tag{3}$$

where F and B are the forward and backward beams, respectively. $D = l\lambda_0/(4\pi n_0 w_0^2)$ corresponds to the diffraction coefficient, where n_0 is the homogeneous refractive index, λ_0 is the laser wavelength in vacuum, l is the length of the crystal, and w_0 the beam waist. z is the propagation coordinate scaled by l. $\Delta_\perp$ is the transverse Laplacian scaled by w_0. Q corresponds to the complex amplitude of the photorefractive reflection grating. τ is the relaxation time related to the photorefractive crystal used. γ represents the photorefractive coupling strength and I_d the background illumination intensity. Similarly to Ref. [18], the boundary condition modeling the feedback and describing the relation between the backward and forward beams at the crystal side facing the mirror is defined as

$$B(z = l) = -\sqrt{R}e^{2ikx\tan(\beta)}\mathcal{F}^{-1}\{e^{2ikL}\mathcal{F}[F(z = l)]\}, \tag{4}$$

where $\mathcal{F}$ is the 2D-transverse Fourrier transform, R the mirror reflectivity ($R = 1$), and β the mirror tilt angle. L is the distance between the mirror and the crystal and k is wave vector. As in the experiment, we inject a Gaussian beam in the (x, y) plane. Numerical simulations are then performed on Eqs. (1)–(3) using a conventional split-step Fourier beam propagation method.

First, the two counterpropagating beams are aligned [no advection effect, $H = 0$, Figs. 2(a),2(b)]. The additional illumination (Fig. 1) is switched off. We work in a range of input powers for which the gain is not saturated. We fix the longitudinal position of the mirror at 1 mm from the back face of the crystal ($L = 1$ mm). For low values of the input power, the system exhibits a homogeneous steady state [Figs. 2(a),2(b)]. By increasing the input power, the pump beam becomes unstable against modulational instability at a specific value of the input power P_{Th}. Above P_{Th}, modulational instability leads to the formation of subcritical honeycomblike patterns (H^- hexagons in the different insets in Fig. 2). Such a subcritical bifurcation scenario leads to a given range of input powers where it is therefore possible to observe a coexistence between the homogeneous steady state and the hexagonal pattern (colored areas in Fig. 2). Similarly to Ref. [9], the hysteresis loop becomes narrower and the threshold power P_{Th} shifts towards larger value when increasing the distance between the feedback mirror and the crystal (not shown here). This is mainly due to the diffraction length in free space between the mirror and the crystal that tends to spread the backward beam and therefore reduces the gain of the two-wave mixing process: the larger the mirror-crystal distance is, the smaller the spatial overlap between the reflected side lobes and the pumped area inside the crystal becomes, therefore increasing the losses. Consequently, for a large crystal-mirror distance, starting from a pattern solution and decreasing the intensity leads quickly to the collapse of the pattern state to the homogeneous solution. Neither the resulting power, nor an eventual underlying dynamics can sustain the upper branch of the hysteresis anymore.

Keeping the mirror-crystal distance constant, we now introduce a weak advectionlike effect by misaligning the feedback mirror [towards the left in Figs. 2(c),2(d)]. The previous stationnary hexagonal pattern is then driven into a drifting dynamics with possibly other geometries. Although different mirror tilt angle ranges give rise to a large variety of pattern geometries [15], we limit our study to the case where the misalignment H is inferior to 10 μm, providing a preferential hexagonal pattern geometry.

Figures 2(c)–2(f) show the dependence of the power in the hexagonal spots versus input beam powers for two different mirror tilts corresponding to a transverse shift $H = 4$ and $H = 8$ μm, respectively. We observe (i) a homogeneous steady state for low values of the input power, and (ii) the modulational instability threshold (P_{Th}) increases as the mirror tilt is increased, i.e., from 0.65 mW for no mirror tilt [Fig. 2(a)] to 1 mW for a medium mirror tilt [Fig. 2(c)] and to 1.45 mW for a strong mirror tilt [Fig. 2(e)]. As explained

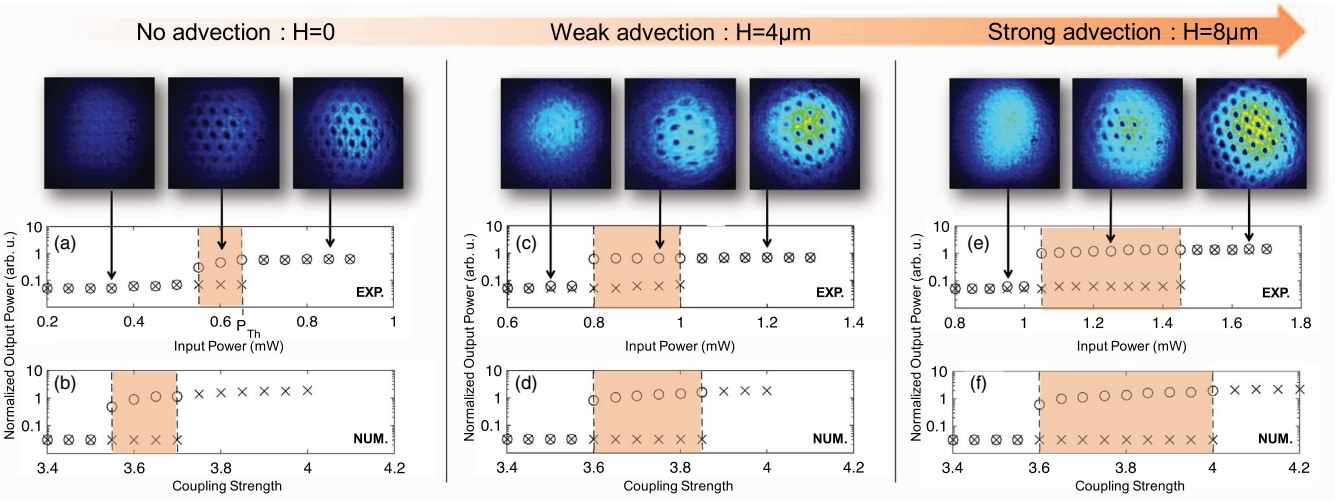

FIG. 2. Normalized intensity of the hexagons as a function of the input power obtained experimentally (EXP.) in (a),(c), and (e) and numerically (NUM.) in (b),(d),(f) as function of the photorefractive coupling strength γ. Crosses and circles are obtained when increasing and decreasing the input power (and corresponding γ), respectively. Three cases are studied: no advection effect (a),(b), weak (c),(d) and strong advection (e),(f) corresponding to a drift of the otherwise stable pattern towards the left on the different pictures. The areas between the dashed lines correspond to the bistability regimes where the homogeneous solution coexists with the hexagonal pattern state. Insets correspond to experimental near-field intensity patterns obtained for different input powers.

earlier for the diffraction path between the feedback mirror and the crystal, the spatial overlap between the reflected side lobes and the pumped area inside the crystal becomes also narrower when we increase the transverse shift between the two counterpropagating beams, thus reducing the photorefractive gain. More power is therefore needed to compensate for the losses. In spite of the losses, surprinsingly, (iii) the bistability range increases as the mirror tilt is increased: from 0.1 mW for $H = 0$ μm to 0.2 mW for $H = 4$ μm, and to 0.4 mW for $H = 8$ μm (similar behaviors with corresponding values of the photorefractive coupling strength γl are shown on the numerical simulations [Figs. 2(b),2(d),2(f)]. Such a counterintuitive result originates from the advection-like effect governed by a peculiar dynamics. This latter may become convective or absolute depending on the input power [15]. Basically, in the so-called convective regime, a perturbation growing on a homogeneous state is simultaneously advected away so that the system returns to the initial homogeneous solution. Theoretically, no pattern arises in this regime. In contrast, in the absolute regime, a disturbance growing locally competes with the drift so that the system reaches a pattern state. The convective regime, where no pattern is expected, can still exhibit patterns if noise is present in the system, which is always the case experimentally. Consequently, macroscopic patterns called noise-sustained structures appear as a result of the amplification in preferential directions of the perturbations produced by the microscopic noise [15,19].

Although experimentally the two regimes lead to pattern formation, in order to distinguish them, one has to look for their specific signatures [15,19,20]. One of the most significant is the area of the near-field intensity pattern inside the available space determined by the size of the pumping area (i.e., the size of the input beam, 300-μm diameter in our experiment). Basically, noise-sustained patterns do not occupy all the modulated space but are located in the area closest to the edge of the outgoing flow (towards the left in our configuration), in contrast to dynamics-sustained patterns (absolute) which invade all the space (see the corresponding pictures for high and medium powers [Figs. 2(c),2(e)]. Finally, the analysis of the size of the near-field patterns enable us to identify the thresholds of the transition from convective to absolute instabilities.

Figure 3 shows the evolution of the pattern size with input power for a strong advection $H = 8$ μm [insets in Figs. 2(e),2(f)]. We chose to analyze the configuration in Figs. 2(e),(f) since it displays the largest bistability range. For low input powers (below 1.3 mW), the output beam shows an homogeneous stationary state. Close to the modulational instability threshold (between 1.3 and 1.4 mW) erratic hexagons appear randomly in time and space with short time duration ("noisy precursor" in Fig. 3). Such a regime is known to be the noisy precursor of the absolute pattern that will grow for higher input powers [20]. In this regime, microscopic noise excites all the possible transverse wave vectors and the newly generated advected pattern has no relation with the one already formed. Regarding the space occupation of the emerging pattern, it occupies in average 90% of the available space. When the input power is still increased between 1.45 and 1.6 mW, drifting hexagons are always present close to the edge of the outgoing flow (see the orange dashed lines compare to the orange solid lines representing the total available

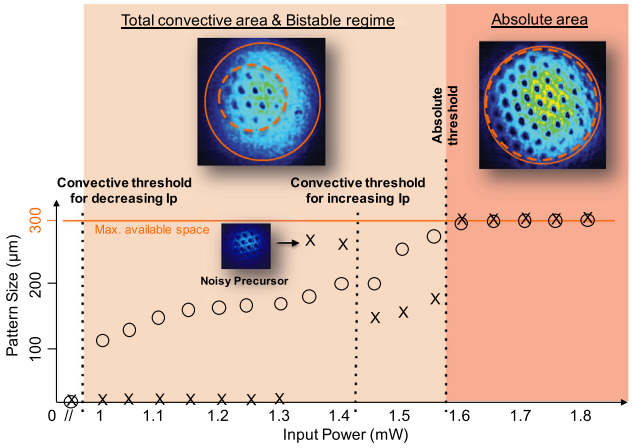

FIG. 3. Evolution of near-field pattern size versus the pump power for a strong advectionlike effect [Figs. 2(e),(f)]. Orange dashed lines correspond to the pattern occupation inside the total available space represented by the solid orange lines. The black dotted lines represent the different thresholds for convective and absolute regimes. Crosses and circles are obtained when increasing and decreasing the input power, respectively.

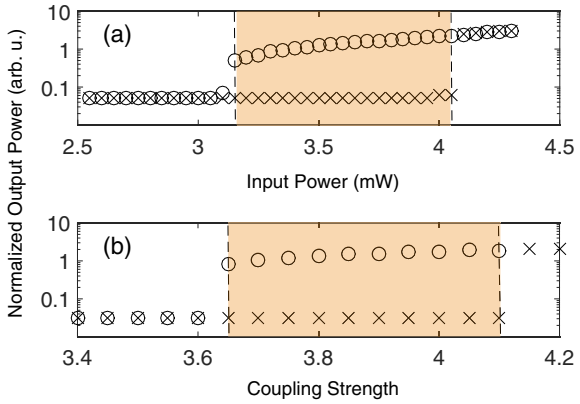

FIG. 4. Plots similar to Figs. 2(e),2(f) with a background illumination switched on. (a) Experimental results and (b) numerical simulation.

space). This localized structure occupies roughly 50% of the pumping area. The perturbations are amplified and advected away but reappear recursively. We are in the presence of convective patterns whose dynamics are sustained by noise. For higher input intensities (above 1.6 mW), the previous convective pattern invades all the available space (Fig. 3, absolute area). Such a phenomenon is connected to a regime where the pattern is sustained by the system dynamics. For decreasing values of the pump power, in the absolute area, the pattern follows the same behavior. The switching point down to the convective area is almost the same ($P = 1.55$ mW) but the pattern maintains its convective dynamics down to 1 mW. The total convective region is therefore directly linked to the bistability area and vice versa. It is worth noting that investigations have been done for other advection parameters and give all similar conclusions.

Finally, we suggest studying the effect of an incoherent background illumination onto the bistability area (Fig. 4). Our starting point corresponds to the largest advectionlike effect [$H = 8\ \mu$m in Figs. 2(e),2(f)]. Similarly to the previous scenario, we show the same measurements as in Figs. 2(e),2(f), but with the background illumination switched on. The intensity of this additional illumination is chosen such as the associated photoconductivities from the pump laser beam (F) and from the incoherent light are comparable. Such an illumination tends to erase the reflection gratings inside the crystal. The losses become higher and the consequence is visible through the shift of the modulational instability threshold towards a higher value ($P_{\mathrm{Th}} = 4.05$ mW compared to 1.45 mW without background illumination; see the corresponding values of γl for numerical simulations). Most importantly, the bistability and corresponding convective region (not shown here but similar to Fig. 3) become larger. Additional thermal effects due to the higher intensity ranges in this configuration generate many other transverse instabilities in the system. Those latter act as a new source of noise that tends to sustain the convective dynamics in a larger intensity scale.

To summarize, in comparison with the classical situation [Figs. 2(a),2(b)] where no background illumination is applied to the PR crystal without any advectionlike effect, we have been able to obtain a 9 times larger bistability region (Fig. 4). We have demonstrated that the bistable regime is directly linked to the convective one where patterns are sustained by noise in the system. Increasing the background illumination and/or the advectionlike effect shifts the modulational instability threshold towards higher intensities. The diffusion associated to the largest intensities acts as a new source of noise that sustains the convective dynamics in a larger intensity scale and, consequently, the bistable area. It is worth mentioning that such observations are interesting in the framework of cavity solitons. One of the crucial mechanisms for the existence of such localized intensity peaks is the presence of an optical bistability between a stable Turing pattern and a homogeneous steady state. Therefore, being able to control the range of parameters where cavity solitons may exist is the key for their generation in nonlinear optical systems. Moreover, our results bring new perspectives into how a nonlinear system behaves in the presence of an advectionlike instability.

The authors acknowledge the Fondation Supélec, the Conseil Régional de Lorraine, Préfecture de Lorraine, and SGAR through the projects PHOTON (FEDER) and APOLLO (FEDER/FNADT), and the Agence Nationale de la Recherche (ANR) TINO Project No. (ANR-12-JS03-005). This work also benefited from the support of the Belgian Science Policy Office under Grant No. IAP-7/35 Photonics@be.

*nicolas.marsal@centralesupelec.fr

[1] L. Lugiato, F. Prati, and M. Brambilla, *Nonlinear Optical Systems* (Cambridge University Press, Cambridge, 2015).
[2] K. Staliunas and V. Sanchez-Morcillo, Springer Tracts Mod. Phys. **183**, 1 (2003).
[3] S. Residori, Phys. Rep. **416**, 201 (2005).
[4] A. Petrossian, M. Pinard, A. Matre, J.-Y. Courtois, and G. Grynberg, Europhys. Lett. **18**, 689 (1992).
[5] T. Ackemann and W. Lange, Phys. Rev. A **50**, R4468 (1994).
[6] T. Honda, Opt. Lett. **18**, 598 (1993).
[7] V. Caullet, N. Marsal, D. Wolfersberger, and M. Sciamanna, Phys. Rev. Lett. **108**, 263903 (2012).
[8] M. Tlidi, P. Mandel, and R. Lefever, Phys. Rev. Lett. **73**, 640 (1994).
[9] S. G. Odoulov, M. Y. Goulkov, and O. A. Shinkarenko, Phys. Rev. Lett. **83**, 3637 (1999).
[10] S. Barland, J. R. Tredicce, M. Brambilla, L. A. Lugiato, S. Balle, M. Giudici, T. Maggipinto, L. Spinelli, G. Tissoni, T. Knodl, M. Miller, and R. Jager, Nature (London) **419**, 699 (2002).
[11] L. A. Lugiato, IEEE J. Quantum Electron. **39**, 193 (2003).
[12] M. Tlidi, K. Staliunas, K. Panajotov, A. G. Vladimirov, and M. G. Clerc, Phil. Trans. R. Soc. A **372**, 20140101 (2014).
[13] M. Tlidi and M. G. Clerc, *Localized Structures in Dissipative Media: From Optics to Plant Ecology*, Springer Proceedings in Physics, Vol. 173 (Springer, New York, 2016).
[14] N. Marsal, L. Weicker, E. Mirisola, D. Wolfersberger, and M. Sciamanna, Proc. SPIE Int. Soc. Opt. Eng. **9894**, 989407 (2016).
[15] N. Marsal, D. Wolfersberger, M. Sciamanna, and G. Montemezzani, Phys. Rev. A **81**, 031804 (2010).
[16] N. Kukhtarev, V. Markov, S. Odulov, M. Soskin, and V. Vinetskii, Ferroelectrics **22**, 949 (1978).
[17] O. Sandfuchs, F. Kaiser, and M. R. Belić, Phys. Rev. A **64**, 063809 (2001).
[18] V. Caullet, N. Marsal, D. Wolfersberger, and M. Sciamanna, Opt. Lett. **38**, 1823 (2013).
[19] M. Santagiustina, P. Colet, M. San Miguel, and D. Walgraef, Phys. Rev. Lett. **79**, 3633 (1997).
[20] A. Mussot, E. Louvergneaux, N. Akhmediev, F. Reynaud, L. Delage, and M. Taki, Phys. Rev. Lett. **101**, 113904 (2008).